The Astrophysical Journal, 739:11 (6pp), 2011 September 20 doi:10.1088/0004-637X/739/1/11

NONTHERMAL EMISSION FROM MIDDLE-AGED SUPERNOVA REMNANTS INTERACTING WITH MOLECULAR CLOUDS

Y. Y. Tang, J. Fang, and L. Zhang
Department of Physics, Yunnan University, Kunming 650091, China; lizhang@ynu.edu.cn
Received 2011 February 6; accepted 2011 June 27; published 2011 August 29

ABSTRACT

Supernova remnants (SNRs) interacting with dense molecular clouds (MCs) are proven to be bright γ-ray emitters by recent observations in the GeV–TeV band. We theoretically investigate the multiband radiative properties of the four middle-aged SNRs IC443, W51C, W28, and W44 with a time-dependent injection model. In the model, part of the SNR shell transports into a dense MC, with the other part of the shell evolving in a relatively tenuous interstellar medium. We find a broken power law with a break energy of ∼3–40 GeV that must be imposed to reproduce the observed multiwavelength spectra for the four remnants. The results indicate that the observed γ-ray spectra can be reproduced as a *p–p* interaction of the high-energy protons injected by the shell interacting with the MC with the dense matter, whereas the radio emission is produced via synchrotron radiation of the injected electrons from the other part of the shell for the four middle-aged SNRs.

Key words: acceleration of particles – ISM: individual objects (IC443, W51C, W28, W44) – ISM: supernova remnants – radiation mechanisms: non-thermal

Online-only material: color figures

1. INTRODUCTION

Recently, GeV gamma-ray emissions from four middle-aged supernova remnants (SNRs) IC443, W51C, W28, and W44 interacting with molecular clouds (MCs) have been detected by the *Fermi* Large Area Telescope (LAT; Abdo et al. 2009, 2010a, 2010b, 2010c). From *Fermi* observations, the gamma-ray spectra of these SNRs indicate broken power-law forms with typical break energies of ∼3–10 GeV and different spectral indices above the break energy. In addition, three of these SNRs are also detected to be emitting TeV gamma-ray emission. These data provide an exciting opportunity to study the emission from the interaction of the SNR with the surrounding matter. Since MCs with high densities are efficient targets of cosmic-ray protons in the SNR–MC interaction system, the clouds illuminated by the protons accelerated in a nearby SNR could be bright gamma-ray sources in which GeV–TeV gamma rays mainly arise from the decay of π^0 produced in inelastic collisions of the accelerated protons with MCs.

Two kinds of models have been proposed to describe gamma-ray emission in the SNR–MC interaction system. The first one assumes that gamma rays produced in MCs result from π^0 decay in the inelastic collisions of the accelerated protons which have escaped from a nearby SNR with MCs and the spectrum of the accelerated protons has a broken power-law form due to the finite size of the emission region (Aharonian & Atoyan 1996; Torres et al. 2008; Gabici et al. 2009; Li & Chen 2010; Ohira et al. 2011). Ohira et al. (2011) applied the model to explain observed gamma-ray spectra in the GeV–TeV energy bands for these four middle-aged SNRs. They found that a runaway-cosmic-ray (CR) spectrum of these SNRs interacting with MCs could be the same, even though it leads to different gamma-ray spectra. On the other hand, Zhang & Fang (2008) proposed a model to explain the observed multiband nonthermal emission of IC443. In this model, an MC is located near the SNR between us and the SNR, a fraction f of the SNR shell evolves in the MC ($f = 1$ means that the whole SNR shell is surrounded by the MC) and the other part evolves in the ambient interstellar environment immediately after supernova explosion (the two parts of the shell evolve independently), and the shell evolves in a uniform medium, i.e., the densities both in the interstellar medium (ISM) and in the MC are constant for simplicity. Zhang & Fang (2008) found that the observed gamma rays are produced both via bremsstrahlung of the shell in the MC and via *p–p* interaction because the high-energy protons interact with the dense matter in the MC, whereas the radio emission from the rim of the SNR is produced via synchrotron radiation in the shell interacting with the ISM.

In the model of Zhang & Fang (2008, hereafter ZF08), a time-dependent nonthermal particle and photon spectra for both young and old shell-type SNRs by including the evolution of secondary $e^{\pm}$ produced via *p–p* interaction when high-energy protons collide with the ambient matter in an SNR (Zhang & Fang 2007; Fang & Zhang 2008) are calculated, where the volume-averaged production rates of the shock-accelerated electrons and protons are the same as those in Sturner et al. (1997), and the total amount of the kinetic energy contained in the injected particles has been completely converted into the kinetic energy of both the electrons and protons during the time up to the radiative stage. However, theoretical investigations show that (1) CRs accelerated at the shock in the partially ionized medium have a broken power-law spectrum, the spectrum above the break energy is steeper than that below the break energy because the damping of waves that resonantly scatter the CRs is significant (Malkov et al. 2011; Inoue et al. 2010), and (2) the accelerated particles at the shock reach their maximum energy near a Sedov stage (Caprioli et al. 2010), so that it is possible that both the electrons and protons obtain their highest kinetic energies during more or less the Sedov stage. Therefore, we make the following modifications to revise the model of Zhang & Fang (2008): (1) the volume-averaged production rates of the shocked-accelerated particles are assumed to have a broken power-law form with a break energy $E_{\rm b}$ and (2) the total amount of the kinetic energy contained in the injected particles has been completely converted into the kinetic energy of both the electrons and protons during the time $t_{\rm ci} = \xi t_{\rm Sed}$

with a parameter $\xi > 10$, where $t_{\rm Sed}$ is the time that the Sedov phase begins. We apply this revised model to these middle-aged SNRs and find out that our results can reproduce the multiband nonthermal spectra of these SNRs under reasonable parameter spaces.

This paper is organized as follows. In Section 2, we review briefly the model of Zhang & Fang (2008) and our modifications to this model. We apply the revised model to these middle-aged SNRs in Section 3. Finally, we give our conclusions and discussion in Section 4.

2. THE MODEL

2.1. Review of the ZF08 Model

In the ZF08 model, three assumptions are made: (1) an MC is located near the SNR between us and the SNR; (2) immediately after supernova explosion, a fraction f of the SNR shell evolves in the MC and other part $(1 - f)$ in the ambient interstellar environment, moreover, the two parts of the shell evolve independently; and (3) the shell evolves in a uniform medium (the ambient ISM or MC). Note that $f = 1$ represents that the whole SNR shell is surrounded by the MC. Under these assumptions, the nonthermal photon spectra from these two parts for the SNR for which a part of the shell ($f < 1$) interacts with the MC are calculated on the frame of the time-dependent model given by Fang & Zhang (2008). However, the value of the factor f would be limited to $f \ll 1$, otherwise the above assumptions will not be valid. Therefore, we change the condition $f < 1$ to $f \ll 1$ or $(1 - f) \ll 1$. In the ZF08 model, the temporal evolution of photon emission from the SNRs is modeled through three parts: the production of accelerated particles by a shock wave, the temporal evolution of particle energy distributions, and the production of photons.

For the production of accelerated particles, the analytical model of the shock dynamics of an SNR with an explosion energy $E = E_{51} \times 10^{51}$ erg expanding at a velocity $v_0 = v_9/10^9$ cm s^{-1} into a uniform ambient medium with density n_0 is used, where $n_0 = \mu n_{\rm ISM}$ and $n_{\rm ISM}$ is the hydrogen density in the local ISM, $\mu = 1.4$ is the mean atomic weight of the ISM assuming 1 helium atom for every 10 hydrogen atoms. The SNR evolves through the free expansion stage which ends at $t = t_{\rm Sed} \approx 2.1 \times 10^2 (E_{51}/n_0)^{1/3} v_9^{5/3})$, the Sedov stage which ends at $t = t_{\rm rad} \approx 4.0 \times 10^4 E_{51}^{4/17} n_0^{-9/17}$ yr, and the radiative stage in which the SNR begins to experience significant radiative cooling (Sturner et al. 1997). The shock velocity $v_{\rm s}(t)$ corresponding to these stages is $v_{\rm s}(t) = v_0$ for $t < t_{\rm Sed}$, $v_{\rm s}(t) = v_0 (t/t_{\rm Sed})^{-3/5}$ for $t_{\rm Sed} \leqslant t < t_{\rm rad}$, and $v_{\rm s}(t) = v_0 (t_{\rm rad}/t_{\rm Sed})^{-3/5} (t/t_{\rm rad})^{-2/3}$ for $t > t_{\rm rad}$. The shock radius is given by $R_s(t) = \int v_{\rm s}(t) dt$.

The volume-averaged production rates of the shock-accelerated electrons and protons are assumed to be

$$Q_i^{\rm pri}(E_i, t) = Q_i^0 G(t) [E_i (E_i + 2 m_i c^2)]^{-[(\alpha+1)/2]} \times (E_i + m_i c^2) \exp(-E_i / E_{i,\rm max}(t)), \quad (1)$$

where $i = e, p$, $G(t)$ is a factor which relates to time, i.e., $G(t) = R_s(t_{\rm Sed})/R_s(t)$ for $t \leqslant t_{\rm rad}$ and $G(t) = 0$ for $t > t_{\rm rad}$, α is the spectral index, and $E_{e,\rm max}$ and $E_{p,\rm max}$ are the maximum energies of the accelerated electrons and protons, respectively. Factors Q_e^0 and Q_p^0 are used to normalize the particle spectra so that the total amount of kinetic energy contained in both the injected electrons and the injected protons is $E_{\rm par} = \eta M_{\rm ej} v_0^2/2$, where $\eta \sim 0.1$ is the efficiency that the kinetic energy of the ejecta with initial mass $M_{\rm ej}$ and initial velocity v_0 is converted into the kinetic energy of both the electrons and the protons. In the estimate of $E_{\rm par}$, a parameter $K_{\rm ep} = Q_e^0/Q_p^0$ is introduced (see Zhang & Fang 2007 for details).

Assuming that an SNR interior is homogeneous, with a constant density $n_{\rm SNR} = 4 n_{\rm ISM}$ and a magnetic field strength $B_{\rm SNR} = 4 B_{\rm ISM}$, $n_e(E_e, t)$ and $n_p(E_e, t)$ are used to represent the differential densities of accelerated electrons and protons, respectively. The direction- and volume-averaged electron intensity $J_e(E_e, t) = (c\beta/4\pi) n_e(E_e, t)$ and proton intensity $J_p(E_p, t) = (c\beta/4\pi) n_p(E_p, t)$ at each moment during the SNR lifetime can be calculated by solving Fokker–Planck equations for both electrons and protons in energy space, which are given by (Zhang & Fang 2007)

$$\frac{\partial n_i(E_i, t)}{\partial t} = -\frac{\partial}{\partial E_i}\left[\dot{E}_i^{\rm tot} n_i(E_i, t)\right] + \frac{1}{2}\frac{\partial^2}{\partial E_i^2}\left[D(E_i, t) n_i(E_i, t)\right] + Q_i(E_i, t) - \frac{n_i(E_i, t)}{\tau_i}, \quad (2)$$

where $i = e, p$, the terms on the right-hand side in Equation (2) represent systematic energy losses, diffusion in energy space, the particle source function, and catastrophic energy loss. It should be noted that the source term for electrons includes the evolution of secondary $e^{\pm}$ produced via p–p interaction when high-energy protons collide with the ambient matter in the SNR, i.e.,

$$Q_e(E, t) = Q_e^{\rm pri} + Q_{e^+}^{\rm sec}(E, t) + Q_{e^-}^{\rm sec}(E, t), \quad (3)$$

where

$$Q_{e^\pm}^{\rm sec}(E, t) = 4\pi \mu_{\rm pp} n_{\rm SNR} \int dE_p J_p(E_p, t) \frac{d\sigma(E_{e^\pm}, E_p)}{dE_{e^\pm}}, \quad (4)$$

where $\mu_{\rm pp}$ is an enhancement factor for collisions involving heavy nuclei in an SNR (Sturner et al. 1997) and $d\sigma(E_{e^-}, E_p)/dE_{e^-}$ and $d\sigma(E_{e^+}, E_p)/dE_{e^+}$ are the differential cross section for electrons and positrons produced via p–p interaction, respectively (Kamae et al. 2006). We solve Equation (1) using a Crank–Nicholson finite difference scheme.

After obtaining the electron intensity $J_e(E_e, t)$ and the proton intensity $J_p(E_p, t)$ at each moment during the SNR lifetime, we can calculate the photon emission from the SNR. The nonthermal radiation processes of the accelerated particles involved in an SNR are synchrotron radiation, bremsstrahlung, inverse Compton scattering (ICS) for leptons including electrons and positrons, and p–p interaction for protons; for the formulae of various radiation processes, see Zhang & Fang (2007).

In this model, model inputs include the distance d and the age T of the source, initial ejecta mass $M_{\rm ej}$, initial shock velocity v_0, the maximum wavelength of magnetohydrodynamic (MHD) turbulence $\lambda_{\rm max}$, conversion efficiency η, electron/proton ratio $K_{\rm ep}$, the spectral index α, hydrogen density $n_{\rm ISM}$ and magnetic field strength $B_{\rm ISM}$ of the ISM, hydrogen density $n_{\rm MC}$ and magnetic field strength $B_{\rm MC}$ of the MC, and the fraction of the shell in the MC f. For each SNR, Equation (2) is respectively solved both with the parameters for the part of the shell evolving in the ISM and with those for the other part interacting with MCs, and then the multiband nonthermal spectra of the two parts can be calculated.

2.2. Revised Version of the ZF08 Model

As mentioned in Section 1, we make two modifications to revise the ZF08 model. The first modification concerns the

volume-averaged production rates of the shocked-accelerated particles. Malkov et al. (2011) proposed a mechanism for the spectral break in the accelerated proton spectrum of an SNR. In this mechanism, the steepening of the energy spectrum of accelerated particles with exactly one power is produced by strong ion–neutral collisions in the surrounding remnant and the spectral break is caused by Alfvén wave evanescence leading to the fractional particle losses (Malkov et al. 2011). Following Malkov et al. (2011), therefore, we assume that the volume-averaged production rates of the shocked-accelerated particles have a broken power-law form with a break energy $E_{\rm b}$, i.e.,

$$Q_i(E,t) = Q_i^0 G(t)(E_i + m_i c^2) \times \begin{cases} \dfrac{[E_i(E_i+2m_ic^2)]^{-[(\alpha_1+1)/2]}}{[E_{\rm b}(E_{\rm b}+2m_ic^2)]^{1/2}}, & E_i \leqslant E_{\rm b}, \\ [E_i(E_i+2m_ic^2)]^{-\frac{\alpha_1+2}{2}} \exp\left(-\dfrac{E_i}{E_{i,\max}(t)}\right), & E_i > E_{\rm b}, \end{cases} \quad (5)$$

where E_i is the particle kinetic energy and α_1 is the spectral index below the break energy $E_{\rm b}$. Malkov et al. (2011) have shown that the break energy (or break momentum) depends on the magnetic field strength and ion density as well as on the frequency of ion–neutral collisions and given an approximate expression of the break momentum; however, the expression cannot make an accurate independent prediction of the position of the break in the gamma-ray emission region since the quantities in the expression are known poorly. As an example, therefore, they used the *Fermi* observations of the gamma-ray spectrum of SNR W44 (Abdo et al. 2010c) to determine the break momentum in the parent particle spectrum. Here, for a given SNR, spectral index α_1 is constrained by observed radio spectral index $\alpha_{\rm r}$ and the break energy $E_{\rm b}$ is determined by the *Fermi* observations.

The second modification is the total amount of the kinetic energy contained in the injected particles that has been completely converted into the kinetic energy of both the electrons and protons during the time $t_{\rm ci} = \xi t_{\rm Sed}$ with a parameter $\xi > 10$, i.e.,

$$E_{\rm par} = \int_0^{t_{\rm ci}} dt\, V_{\rm SNR}(t) \times \left[\int_0^{E_{\rm e,max}} dE\, E\, Q_e(E,t) + \int_0^{E_{p,\max}} dE E Q_p(E,t)\right], \quad (6)$$

where $V_{\rm SNR}(t) = 4\pi R_{\rm SNR}^3(t)/3$ is the SNR volume.

After making the above modifications, we can numerically calculate the isotropic intensities of the primary electrons, the primary protons, and the secondary $e^{\pm}$ pairs in the shell evolving in the ISM and in the shell interacting with the MC for a given SNR. The intensity is cut off at high energies by three mechanisms: the finite age of the SNR, energy-loss processes, and free escape from the shock region when the particles cannot be effectively scattered by MHD turbulence (Gaisser 1990; Reynolds 1996; Sturner et al. 1997). Particularly with MHD turbulence, a turbulent maximum wavelength is described as $\lambda_{\max} = f_0 r_L$ ($f_0 \sim 10$; see Zhang & Fang 2007); here, $r_L = E_i/eB$ is the particle gyroradius and B is the local magnetic field strength. Through these mechanisms, the maximum kinetic energies of electrons and protons, $E_{e,\max}$ and $E_{p,\max}$, can be calculated with Equations (3)–(5) in Zhang & Fang (2007), which depend on the shock speed and age as well as on any of the above-mentioned loss processes.

Table 1
Model Parameters in Our Calculations

Model Parameter	IC443	W51C	W28	W44
T (10^4 yr)	3.0	3.5	4.0	2.0
d (kpc)	1.5	6.0	2.0	3.0
$M_{\rm ej}$ ($M_\odot$)	1.5	6.0	3.0	6.0
$B_{\rm ISM}$ (μG)	10	25	10	10
$n_{\rm MC}$ (cm^{-3})	50	100	100	100
$B_{\rm MC}$ (μG)	10	25	10	10
$K_{\rm ep}$	0.012	0.012	0.01	0.01
ξ	90	55	70	36
α_1	1.7	1.5	1.7	2.0
$E_{\rm b}$ (GeV)	40	10	3	10
f	0.08	0.15	0.12	0.10

Notes. In our calculations, we assume the same values of the initial velocity v_0, conversion factor η, the maximum wavelength of MHD turbulence $\lambda_{\max}$, and local ISM density $n_{\rm ISM}$ for these SNRs: $v_0 = 1.0 \times 10^9$ cm s^{-1}, $\eta = 0.1$, $\lambda_{\max} = 5.0 \times 10^{16}$ cm, and $n_{\rm ISM} = 0.1$ cm^{-3}.

In the revised model, we calculate nonthermal photon spectra by using the accelerated electron and proton intensities with a broken power-law particle injection. These photons can be produced by electron synchrotron radiation, bremsstrahlung, ICS, and neutral π^0-decay gamma rays from the proton–proton interaction. The ambient soft photon fields of the ICS include the cosmic microwave background (CMB), Galactic IR emission from the warm dust, and the Galactic starlight field (Porter et al. 2008). The detailed process of the photon emission is shown in Fang & Zhang (2008). Based on Kamae et al. (2006), the gamma-ray spectrum of π^0 decay is calculated with a new scaling factor of 1.85 for helium and other heavy nuclei (Mori 2009).

3. APPLICATIONS

In this section, we apply the model to four middle-aged SNRs IC443, W51C, W28, and W44 interacting with the surrounding MC. The model parameters used in our calculations for these SNRs are listed in Table 1, where the initial shock velocity v_0, conversion efficiency η, the maximum wavelength of MHD turbulence $\lambda_{\max}$, local ISM density $n_{\rm ISM}$, and MC hydrogen density $n_{\rm MC}$ are fixed to be 10^9 cm s^{-1}, 0.1, 5×10^{16} cm, and 0.1 cm^{-3} respectively for these SNRs. The comparisons of our calculating results with observed data are shown in Figures 1–4. In these figures, we indicate nonthermal photon spectra through various radiation mechanisms under the circumstances that the SNR shock interacts with the ISM: the dashed, dot-dashed, and dotted lines represent the spectra through synchrotron emission, ICS, and bremsstrahlung, respectively; double-dot-dashed lines express the spectra from π^0-decay process; and thin solid lines represent the summation of all the above processes in the ISM. For the clarity of the figure, only the summation for all the above-mentioned radiations from the shock shell interacting with the MCs is shown (thick solid lines), whereas the individual radiative spectrum, such as synchrotron radiation, bremsstrahlung, ICS, and neutral π^0-decay emission from the part interacting with the MCs, is not given in these figures.

SNR IC443 is a well-studied shell-type SNR with age 20–30 kyr (Bykov et al. 2008; Lee et al. 2008); it is located at a distance of 1.5 kpc (Gaensler et al. 2006) and listed as the core-collapse SNR G189.1+3.0 in Green's catalog (Green 2004). There is a complex composition of molecular and atomic clouds in the southern rim of the shell (Snell et al. 2005). The multiband

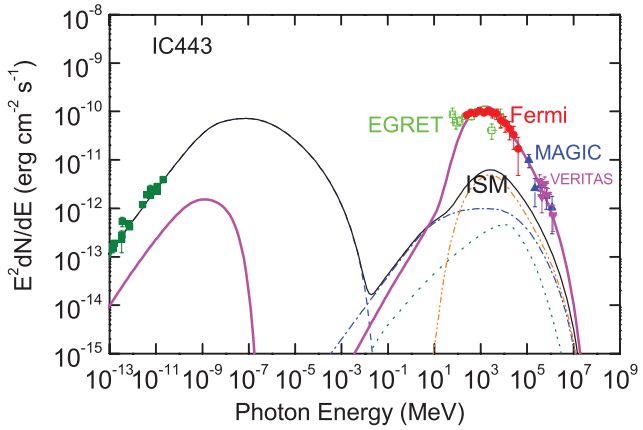

Figure 1. Comparison of the predicted SEDs with the observed data for SNR IC443. The radio emission (from Erickson et al. 1985) is explained by synchrotron radiation from the SNR shock evolving in the ISM, while the gamma-ray emission is from the combinations of bremsstrahlung (dotted line), IC scattering (dot-dashed line), and π^0-decay (double-dot-dashed line) owing to the SNR shock interacting with MC. Gamma-ray data are released by the EGRET (Hartman et al. 1999), *Fermi* LAT (Abdo et al. 2010a), MAGIC (Albert et al. 2007), and VERITAS (Acciari et al. 2009). Details of the model are described in the text.

(A color version of this figure is available in the online journal.)

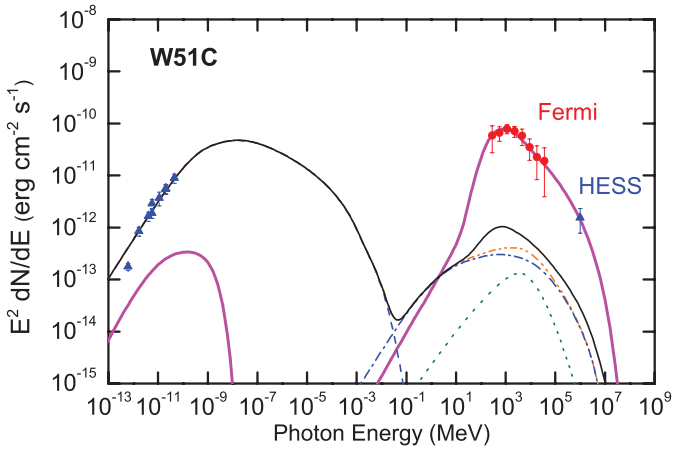

Figure 2. Comparison of the predicted SEDs with the observed data for SNR W51C. All the curves are stated to be the same as in the caption of Figure 1. The physical parameters are shown in Table 1. The multiband data are from the observations in radio (Moon & Koo 1994) and high-energy gamma rays (Abdo et al. 2009). Details of the models are described in the text.

(A color version of this figure is available in the online journal.)

data have been obtained at radio (Erickson et al. 1985), GeV gamma-ray (Esposito et al. 1996; Hartman et al. 1999; Abdo et al. 2010a), and VHE gamma-ray (Albert et al. 2007; Acciari et al. 2009) bands; specifically, the VHE gamma rays observed by MAGIC are correlated with an MC (Albert et al. 2007), and the total mass of the MC in the region is estimated to be $\sim 10^4\ M_\odot$ (Torres et al. 2003). We calculate the multiband spectral energy distribution (SED) of IC443 using our revised model and show the comparison of our results with observed radio data (Erickson et al. 1985), EGRET data (Hartman et al. 1999), *Fermi* LAT data (Abdo et al. 2010a), and VHE data detected by MAGIC (Albert et al. 2007) and VERITAS (Acciari et al. 2009) in Figure 1. The parameters involved in the calculation are shown in Table 1. In our calculation, we assume that the radio photons are produced by the synchrotron radiation of the accelerated electrons, so we can estimate the spectral index $\alpha_1 = 1$–$2\alpha_r$ by using the observed radio spectral index, from the radio observations, $\alpha_r = -0.36 \pm 0.2$ (e.g., Erickson et al. 1985), so $\alpha_1 \approx 1.7$; on the other hand, we use the *Fermi* observations to estimate E_b and find $E_b = 40$ GeV. Therefore, we have the broken power-law form of the volume-averaged production rates of the shocked-accelerated particles with $\alpha_1 = 1.7$ and $E_b = 40$ GeV. With the parameter $\xi = 90$ listed in Table 1, we find that $t_{ci} \approx 41{,}270$ years when the shell evolves in the ISM, and $t_{ci} \approx 5200$ years for the shell interacting with the MC, indicating that the total amount of the kinetic energy contained in the injected particles could be more quickly converted into the kinetic energy of both the electrons and protons in the dense MC than that in the ISM. The soft photon fields of ICS include the CMB, Galactic IR emission from the warm dust, and the Galactic starlight field (two optical blackbody components); the temperatures and energy densities of these photon fields are 2.7, 25, 5000, and 10,000 K and $U_{CMB} = 2.5 \times 10^{-7}$ MeV cm^{-3}, $U_{IR} = 2.2 \times 10^{-7}$ MeV cm^{-3}, $U_{5000} = 2.2 \times 10^{-7}$ MeV cm^{-3}, and $U_{10,000} = 2.2 \times 10^{-7}$ MeV cm^{-3}, respectively (Sturner et al. 1997). Moreover, $K_{ep} = 0.01$ is used in our calculation which is approximately consistent with the CR composition observed at Earth (Abdo et al. 2010c). Note that gamma-ray emissivity for the bremsstrahlung and p–p interaction in the MC is proportional to $f \times n_{MC}$ when the value of t_{ci} is fixed in the MC. Therefore, in order to produce the gamma-ray spectrum which can be comparable to the observed data, increasing n_{MC} leads to decreasing f with a fixed t_{ci}. Here, $f = 0.08$ and $n_{MC} = 50$ cm^{-3} are used, if we fix the value of t_{ci} in the MC, obviously a higher or lower value of n_{MC} is possible to reproduce the observed data if a lower or higher value of f is used. From our calculation, the radio emission from the rim of the SNR is produced by the radiation from the shell evolving in the ISM, whereas the gamma rays detected by EGRET, *Fermi* LAT, MAGIC, and VERITAS are prominently from the π^0 decay of the shell interacting with the MC.

SNR W51C (G49.2-0.7) is a radio-bright SNR with an estimated age of $\sim 3.5 \times 10^4$ yr at a distance of $D \simeq 6$ kpc (Koo et al. 2005). Koo & Moon (1997a, 1997b) have given evidence of MC-shock interaction. X-ray observations by *ROSAT*, *ASCA*, and *Chandra* indicate intense radio synchrotron emission in its shell and both shell-type and center-filled morphologies. An age of $\sim 3 \times 10^4$ yr and an explosion energy of $\sim 3.6 \times 10^{51}$ erg for this SNR were estimated based on either the Sedov or the evaporative models (Koo et al. 1995). In the TeV gamma-ray band, an extended source HESS J1923+141 coincident with W51C has been found using HESS (Fiasson et al. 2009). In the GeV gamma-ray band, bright gamma-ray emission from W51C was observed (Abdo et al. 2009) and known to be interacting with an MC. The gamma-ray emission is spatially extended, broadly consistent with the radio and X-ray extent of W51C. Abdo et al. (2009) took into account constant particle injection over a period of $\sim 3 \times 10^4$ yr, and they found that the large luminosity of the shocked shell could be explained naturally by π^0 decay with a large number of accelerated protons in dense environments. The initial mass of the ejecta for W51C is considered as $\sim 6\ M_\odot$. We calculate the multiband SED of W51C using our revised model and show the comparison of our results with observed radio data (Moon & Koo 1994), *Fermi* LAT data (Abdo et al. 2009), and VHE data detected by HESS (Fiasson et al. 2009) in Figure 2. In our calculation, α_1 is constrained to be 1.5 by using $\alpha_r \approx -0.25$ and E_b is constrained to 10 GeV by using the *Fermi* observations. The interstellar radiation fields for ICS include the CMB and two diluted blackbody components (IR and optical); the temperatures are shown as $T_{IR} = 2.7$ K, $T_{IR} = 35$ K, and

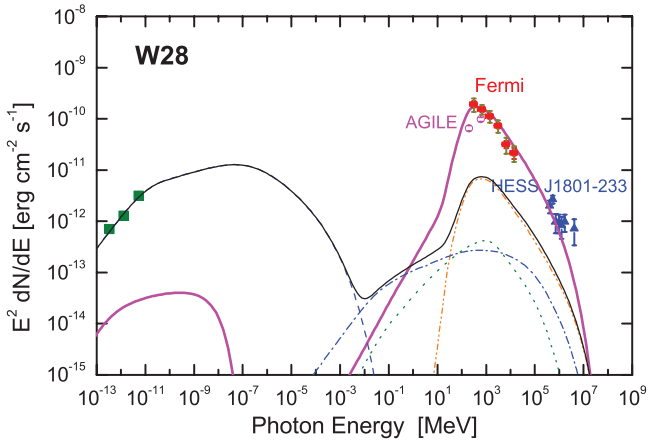

Figure 3. Comparison of the predicted SEDs with the observed data for SNR W28. The multiband data are from the observations in radio (Dubner et al. 2000) and high-energy gamma rays (Aharonian et al. 2008; Giuliani 2010; Abdo et al. 2010b). Details of the models are described in the text.

(A color version of this figure is available in the online journal.)

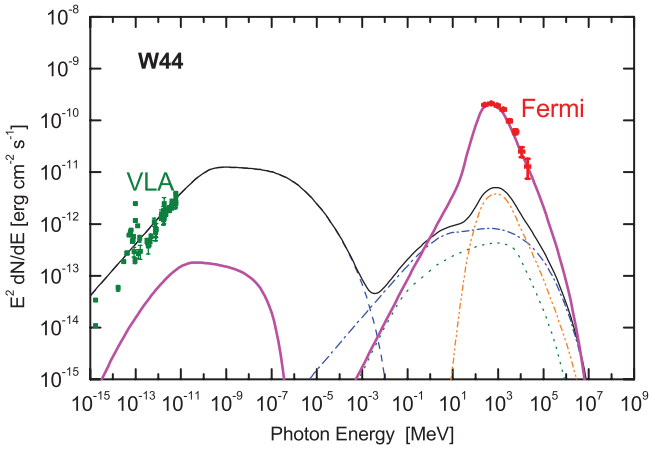

Figure 4. Comparison of the predicted SEDs with the observed data for the SNR W44. The multiband data are from the observations in radio (Castelletti et al. 2007) and high-energy gamma rays (Abdo et al. 2010c). Details of the models are described in the text.

(A color version of this figure is available in the online journal.)

$T_{\rm IR} = 2900$ K, corresponding to $U_{\rm CMB} = 2.6\times10^{-7}$ MeV cm^{-3}, $U_{\rm IR} = 9.0\times10^{-7}$ MeV cm^{-3}, and $U_{\rm opt} = 8.4\times10^{-7}$ MeV cm^{-3}, respectively (Porter et al. 2008; Abdo et al. 2009). We find that $\xi = 55$, which gives $t_{\rm ci} \approx 40{,}039$ years in the ISM and $t_{\rm ci} \approx 4004$ years in the dense MC with $f = 0.15$. From our calculation, the gamma ray is also explained as the contribution from the π^0 decay of accelerated protons in dense MC. Correspondingly, the radio emission is from the shell interacting with the ISM.

SNR W28 (G6.4-0.1) has a mixed morphology characterized by a shell-like radio morphology and center-filled thermal X-ray emission, and located at a distance of ∼2 kpc; its age varies between 3.5 and 15 × 10^4 yr (Kaspi et al. 1993), here we take its age as 4.0 × 10^4 yr. Dubner et al. (2000) have shown that the shell-like radio radiation should be prominently from its northeastern region. The X-ray emission is from the northeast and southwest, and it also shows a limb-brightened shell morphology (Rho & Borkowski 2002). HESS observations of the W28 field have revealed four TeV gamma-ray sources coincident with MCs (Aharonian et al. 2008): HESS J1801−233 located along the northeastern boundary coincides with an MC interacting with W28, and other three sources, HESS J1800−240A, B, and C, located at the south of W28. *Fermi* LAT observed gamma-ray emission from two gamma-ray sources, 1FGL J1801.3−2322c and 1FGL J1801.3−2322c. The source 1FGL J1801.3−2322c is an extended source within the northeastern boundary of SNR W28, and extensively overlaps with the TeV gamma-ray source HESS J1801−233. Here we model the multiband emission from this region; the soft photon fields for ICS include the CMB, two infrared ($T_{\rm IR} = 29,490$ K, $U_{\rm IR} = 2.9\times10^{-7}$, 5.3×10^{-8} MeV cm^{-3}, respectively), and two optical components ($T_{\rm IR} = 3600$, 10,000 K, $U_{\rm opt} = 3.7\times10^{-7}$, 1.3×10^{-7} MeV cm^{-3}, respectively; Porter et al. 2008; Abdo et al. 2010b). In Figure 3, we show the comparison of our results with observed radio data (Dubner et al. 2000), *Fermi* LAT data (Abdo et al. 2010b), and VHE data detected by HESS (Aharonian et al. 2008). In order to reproduce the observed multiband spectrum, we obtain $\alpha_1 = 1.7$ from the observed radio spectral index $\alpha_{\rm r} \approx -0.35$ and $E_{\rm b} = 3$ GeV from the *Fermi* observations. Moreover, $\xi = 70$ for this SNR, resulting in $t_{\rm ci} \approx 40{,}446$ years in the ISM and $t_{\rm ci} \approx 4045$ years in the MC environment.

SNR W44 (G34.7-0.4) is also a radio-bright SNR; over the age of the SNR (2 × 10^4 yr) with a mixed morphology, it is located in a complex region at a distance of ∼3 kpc. Castelletti et al. (2007) performed low-frequency observations of SNR W44 at 74 and 324 MHz using multiple configurations of the Very Large Array (VLA); the observation of W44 has shown a highly filamentary radio shell and centrally concentrated thermal X-ray emission, and there was no correlation found between the associated pulsar PSR B1853+01 and the surrounding SNR shell by analyzing the radio continuum spectrum. However, the brightest X-ray features located in the center region of the remnant are relative to low radio surface brightness (Rho & Petre 1998). The gamma-ray emission spatially associates with W44, and existing studies have shown that the SNR shock should be interacting with an external MC (Abdo et al. 2010c). We calculate the multiband SED of W44 using our revised model and show the comparison of our results with observed radio data (Castelletti et al. 2007) and *Fermi* LAT data (Abdo et al. 2010c) in Figure 4. The seed photons for ICS include infrared radiation with energy density of 9.3 × 10^{-7} MeV cm^{-3}, optical radiation with 9.6 × 10^{-7} MeV cm^{-3}, and the CMB with 2.6 × 10^{-7} MeV cm^{-3} as well as infrared photons from W44 itself with 6.9 × 10^{-7} MeV cm^{-3} (de Jager & Mastichiadis 1997; Abdo et al. 2010c). The model parameters are listed in Table 1. In order to reproduce the observed data, $\alpha_1 = 2.0$ since $\alpha_{\rm r} \approx -0.5$ and $E_{\rm b} = 10$ GeV from the *Fermi* observations, i.e., a steep power-law injection above $E_{\rm b}$ is required. With $\xi = 36$ for this source, we have $t_{\rm ci} \approx 26{,}207$ years in the ISM and $t_{\rm ci} \approx 2621$ years in the MC environment.

4. SUMMARY AND DISCUSSION

In this paper, we have revised the model of nonthermal photon emission from a shell-type SNR with part of the shell interacting with an MC given by Zhang & Fang (2008) and then applied the model for four middle-aged SNRs IC443, W51C, W28, and W44. In this revised model, we assumed a broken power-law particle injection by assuming that the injected electrons have the same energy distribution as the protons, and that the total amount of the kinetic energy contained in the injected particles were completely converted into the kinetic energy of both the electrons and protons during the time $\xi t_{\rm Sed}$. The nonthermal photon emission consists of two components:

one comes from the shell evolving in the ISM and another from the MC. The main conclusion is that the observed GeV–TeV gamma rays are produced both via the bremsstrahlung of the shell in the MC and via the p–p interaction because the high-energy protons interact with the ambient matter in the MC whereas the radio emissions from the rim of the SNRs are produced via synchrotron radiation in the shell interacting with the ISM.

In our calculations, we found that $K_{\rm ep} \sim 0.01$ for these SNRs which is approximately consistent with the CR composition observed on Earth. Before the observations of *Fermi* LAT, the study of multiband (from radio to GeV–TeV bands) emission for the SNR interacting with MCs mainly focused on SNR IC443 since this SNR has been observed from the radio (Erickson et al. 1985) to GeV–TeV bands by EGRET (Hartman et al. 1999) and MAGIC (Albert et al. 2007). For example, Sturner et al. (1997) calculated the nonthermal spectra from IC443 in the ambient medium with $n_{\rm ISM} = 10$ and $n_{\rm ISM} = 1$ cm^{-3}, respectively, by using a time-dependent SNR model with $K_{\rm ep} = 0.625$ and concluded that the synchrotron emission dominates in the radio band and the bremsstrahlung in the gamma-ray band (i.e., the contribution of the p–p collision to gamma rays is negligible). Bykov et al. (2000) proposed a model to describe the nonthermal emission from an SNR which is fully surrounded by the MC and applied to SNR IC443 and predicted that the spectrum has a sharp cutoff at ∼0.1 TeV which is not consistent with the observation. Zhang & Fang (2008) reproduced an observed multiband spectrum of SNR IC443 using the ZF08 model with the $K_{\rm ep} = 0.1$, which is larger than the observed value. For the other three SNRs, a simple model with a broken power-law particle injection can explain multiband nonthermal photon emissions (Abdo et al. 2009, 2010b, 2010c), where $K_{\rm ep} \sim 0.01$ is used. For the model parameters, the maximum turbulence scale is the same for all four sources, the values (see Table 1) of the spectral index α_1 of the broken power law can be estimated from the observed data in the radio band ($\alpha_{\rm r} = -0.36 \pm 0.02$ for IC443 (Erickson et al. 1985), $\alpha_{\rm r} \approx -0.26$ for W51C (Moon & Koo 1994), $\alpha_{\rm r} \approx -0.35$ for W28 (Dubner et al. 2000), and $\alpha_{\rm r} \approx -0.5$ for W44 (Castelletti et al. 2007)), and the break energy $E_{\rm b}$ can be constrained by the gamma-ray spectrum for a certain SNR (Abdo et al. 2009, 2010a, 2010b, 2010c). However, it is very difficult to accurately determine all physical parameters; future observation is expected to give more accurate model parameters.

The values of the factor f of the shell in the MC were adopted as 0.08, 0.15, 0.12, and 0.10 for SNRs IC443, W51C, W28, and W44, respectively, i.e., there is ∼10% of the SNR shell interacting with the MC for these four SNRs. When high-energy particles interact with the surrounding dense MC, two emission processes become very important: π^0-decay gamma rays in p–p interaction and electron bremsstrahlung. The parameters $n_{\rm MC}$ and f are certainly important to these two mechanisms, and $f \times n_{\rm MC}$ is proportional to the gamma-ray emissivity. A reasonable value of $f \times n_{\rm MC}$ should be given in order to reproduce gamma-ray spectra consistent with the observed data, thus increasing f can result in decreasing $n_{\rm MC}$ on the condition that the value of $t_{\rm ci}$ is fixed in the MC and vice versa.

Finally, we would like to point out that although our model can reproduce the multiband spectral energy distributions from four middle-aged SNRs interacting with MCs, another kind of model that gamma rays produced in MCs results from π^0 decay in the inelastic collisions of the accelerated protons which have escaped from a nearby SNR with MCs can also explain the GeV–TeV emission observed by *Fermi* LAT well (Torres et al. 2008; Gabici et al. 2009; Li & Chen 2010; Ohira et al. 2011). Therefore, further observed information are required to further understand the emission processes of these SNRs.

We thank the anonymous referee for very constructive comments that substantially improved the quality of this paper. This work is partially supported by the National Natural Science Foundation of China (NSFC 10778702, 10803005), a 973 Program (2009CB824800), the Foundation of Yunnan University (21132014, 2010YB043), and Yunnan Province under a grant 2009 OC.

REFERENCES

Abdo, A. A., Ackermann, M., Ajello, M., et al. 2009, ApJ, 706, L1
Abdo, A. A., Ackermann, M., Ajello, M., et al. 2010a, ApJ, 712, 459
Abdo, A. A., Ackermann, M., Ajello, M., et al. 2010b, ApJ, 718, 348
Abdo, A. A., Ackermann, M., Ajello, M., et al. 2010c, Science, 327, 1103
Acciari, V. A., Aliu, E., Arlen, T., et al. 2009, ApJ, 698, L133
Aharonian, F., Akhperjanian, A. G., Bazer-Bachi, A. R., et al. 2008, A&A, 481, 401
Aharonian, F. A., & Atoyan, A. M. 1996, A&A, 309, 917
Albert, J., Aliu, E., Anderhub, H., et al. 2007, ApJ, 664, L87
Bykov, A. M., Chevalier, R. A., Ellison, D. C., & Uvarov, Yu. A. 2000, ApJ, 538, 203
Bykov, A. M., Krassilchtchikov, A. M., Uvarov, Yu. A., et al. 2008, ApJ, 676, 1050
Caprioli, D., Amato, E., & Blasi, P. 2010, Astropart. Phys., 33, 160
Castelletti, G., Dubner, G., Brogan, C., & Kassim, N. E. 2007, A&A, 471, 537
de Jager, O. C., & Mastichiadis, A. 1997, ApJ, 482, 874
Dubner, G. M., Velázquez, P. F., Goss, W. M., & Holdaway, M. A. 2000, AJ, 120, 1933
Erickson, W. C., & Mahoney, M. J. 1985, ApJ, 290, 596
Esposito, J. A., Hunter, S. D., Kanbach, G., & Sreekumar, P. 1996, ApJ, 461, 820
Fang, J., & Zhang, L. 2008, MNRAS, 384, 1119
Fiasson, A., Marandon, V., Chaves, R. C. G., & Tibolla, O. (The H.E.S.S. Collaboration). 2009, in Proc. 31st ICRC (Lodz), in press
Gabici, S., Aharonian, F. A., & Casanova, S. 2009, MNRAS, 396, 1629
Gaensler, B. M., Chatterjee, S., Slane, P. O., et al. 2006, ApJ, 648, 1037
Gaisser, T. K. 1990, Cosmic Rays and Particle Physics (Cambridge: Cambridge Univ. Press)
Giuliani, A. 2010, A&A, 516, L11
Green, D. A. 2004, Bull. Astron. Soc. India, 32, 335
Hartman, R. C., Bertsch, D. L., Bloom, S. D., et al. 1999, ApJS, 123, 79
Inoue, T., Yamazaki, R., & Inutsuka, S. 2010, ApJ, 723, L108
Kamae, T., Karlsson, N., Mizuno, T., Abe, T., & Koi, T. 2006, ApJ, 647, 692
Kaspi, V. M., Lyne, A. G., Manchester, R. N., et al. 1993, ApJ, 409, L57
Koo, B.-C., Kim, K.-T., & Seward, F. D. 1995, ApJ, 447, 211
Koo, B.-C., Lee, J.-J., Seward, F. D., & Moon, D.-S. 2005, ApJ, 633, 946
Koo, B.-C., & Moon, D.-S. 1997a, ApJ, 475, 194
Koo, B.-C., & Moon, D.-S. 1997b, ApJ, 485, 263
Lee, J.-J., Koo, B.-C., Yun, M. S., et al. 2008, AJ, 135, 796
Li, H., & Chen, Y. 2010, MNRAS, 409, 35
Malkov, M. A., Diamond, P. H., & Sagdeev, R. Z. 2011, Nat. Commun., 2, 194
Moon, D.-S., & Koo, B.-C. 1994, J. Korean Astron. Soc., 27, 81
Mori, M. 2009, Astropart. Phys., 31, 341
Ohira, Y., Murase, K., & Yamazaki, R. 2011, MNRAS, 410, 1577
Porter, T. A., Moskalenko, I. V., Strong, A. W., Orlando, E., & Bouchet, L. 2008, ApJ, 682, 400
Reynolds, S. P. 1996, ApJ, 459, L13
Rho, J., & Borkowski, K. J. 2002, ApJ, 575, 201
Rho, J., & Petre, R. 1998, ApJ, 503, L167
Snell, R. L., Hollenbach, D., Howe, J. E., et al. 2005, ApJ, 620, 758
Sturner, S. J., Skibo, J. G., Dermer, C. D., & Mattox, J. R. 1997, ApJ, 490, 619
Torres, D. F., Rodriguez Marrero, A. Y., & de Cea Del Pozo, E. 2008, MNRAS, 387, 59
Torres, D. F., Romero, G. E., Dame, T. M., Combi, J. A., & Butt, Y. M. 2003, Phys. Rep., 382, 303
Zhang, L., & Fang, J. 2007, ApJ, 666, 247
Zhang, L., & Fang, J. 2008, ApJ, 675, L21 (ZF08)